

Original Article

Open Access



Gene editing treatment strategies for retinitis pigmentosa assessed in *Xenopus laevis* carrying a mutant Rhodopsin allele

Farhad Ghaseminejad¹, Beatrice M. Tam¹, Colette N. Chiu¹, Joanna M. Feehan^{1,2}, Orson L. Moritz¹

¹Department of Ophthalmology & Visual Sciences, University of British Columbia, UBC/VGH Eye Care Centre, Vancouver, BC V5Z 3N9, Canada.

²Current affiliation: The Sainsbury Laboratory, University of East Anglia, Norwich NR4 7UH, UK.

Correspondence to: Orson L. Moritz, Department of Ophthalmology & Visual Sciences, University of British Columbia, UBC/VGH Eye Care Centre, 2550 Willow Street, Vancouver, BC V5Z 3N9, Canada. E-mail: olmoritz@mail.ubc.ca

How to cite this article: Ghaseminejad F, Tam BM, Chiu CN, Feehan JM, Moritz OL. Gene editing treatment strategies for retinitis pigmentosa assessed in *Xenopus laevis* carrying a mutant Rhodopsin allele. *J Transl Genet Genom* 2022;6:111-25. <https://dx.doi.org/10.20517/jtgg.2021.49>

Received: 28 Sep 2021 **First Decision:** 8 Nov 2021 **Revised:** 26 Nov 2021 **Accepted:** 9 Dec 2021 **Published:** 17 Feb 2022

Academic Editor: Bernhard H. F. Weber **Copy Editor:** Yue-Yue Zhang **Production Editor:** Yue-Yue Zhang

Abstract

Aim: To examine the utility of gene editing therapies for retinitis pigmentosa using *Xenopus laevis* carrying a mutation in *Rhodopsin*.

Methods: *Xenopus laevis* were genetically modified using CRISPR-Cas9 based methods and characterized by Sanger sequencing, dot blot, electroretinography, and confocal microscopy.

Results: We identified genetically modified *Xenopus laevis* carrying a net 12 base pair deletion in the *Rho.L* gene. These animals have a retinal degeneration that is apparent by 14 days, with abnormal or missing rod outer segments, and a reduced electroretinogram signal. We prevented the majority of this retinal degeneration via a treatment strategy using a single sgRNA to neutralize the mutant allele via non-homologous end joining, yielding long-term improvements in histology and the electroretinogram. A second strategy using two sgRNAs to generate large deletions in the mutant allele was also successful, but did not significantly improve outcomes relative to the single-guide strategy as it was less efficient. We found limited evidence of success with a third strategy dependent on homology-directed repair; this treatment was also too inefficient to generate an outcome superior to the single-guide strategy.



© The Author(s) 2022. **Open Access** This article is licensed under a Creative Commons Attribution 4.0 International License (<https://creativecommons.org/licenses/by/4.0/>), which permits unrestricted use, sharing, adaptation, distribution and reproduction in any medium or format, for any purpose, even commercially, as long as you give appropriate credit to the original author(s) and the source, provide a link to the Creative Commons license, and indicate if changes were made.



Conclusion: Our results demonstrate the utility of this new *Xenopus laevis* model for rapidly assessing and comparing multiple gene-editing based treatment strategies. We conclude that it would be technically difficult to improve on the simple single-guide based strategy, as strategies requiring multiple successive events (such as cleavage followed by homology-directed repair) are likely to be less efficient.

Keywords: Rhodopsin, autosomal dominant retinitis pigmentosa, CRISPR/Cas9, gene editing, gene therapy

INTRODUCTION

Retinitis pigmentosa (RP) is a vision-threatening disorder characterized by loss of functional and viable photoreceptors and retinal degeneration (RD)^[1]. RP affects 1 in 3500-4500 people worldwide, making it one of the most common inherited retinal diseases^[2]. RP is rod-cone dystrophy, in which initial symptoms of night blindness associated with rod degeneration progress to secondary cone death, resulting in the loss of daylight peripheral vision, potentially leading to complete blindness^[3].

Although most cases of RP are monogenic, thousands of different mutations in more than 50 genes underlie this disorder^[4]. This genetic heterogeneity has made treatment development complex, and RP is untreatable for more than a million affected individuals worldwide^[5]. In 30%-40% of cases, RP is inherited as an autosomal dominant trait (adRP)^[5]. Notably, 25% of adRP cases stem from mutations in the rhodopsin gene (*RHO*), making *RHO* mutations the most common cause of adRP. To date, more than 150 distinct missense/nonsense *RHO* mutations have been associated with adRP^[6]. Mutations in *RHO* can also cause recessive RP; in these cases, the mutations are typically null alleles^[6,7].

CRISPR/Cas9 is a two-component gene editing system found in bacteria species that has been co-opted by molecular biologists to permit a diverse range of genetic manipulations^[8]. The CRISPR/Cas9 complex is made up of a DNA-cleaving enzyme called Cas9 and an RNA molecule that guides Cas9 to a specific target site, referred to as single-guide RNA (sgRNA)^[9]. SgRNAs recognize unique ~20 nucleotide target sequences flanked by a protospacer-adjacent motif (PAM) e.g., NGG in the case of *S. pyogenes* Cas9^[10]. Cas9 introduces double-strand breaks 3bp upstream from the PAM site. When the CRISPR/Cas9 system is employed in vertebrate cells, the resulting DNA cleavage initiates either non-homologous end joining (NHEJ) or homology-directed recombination (HDR) DNA repair pathways^[11]. NHEJ is an error-prone response that results in insertions and deletions (indels) of short DNA sequences at the break site. Within *RHO* genes, NHEJ can create frame-shifting indels that promote nonsense-mediated decay (NMD) of the mRNA, generating loss-of-function mutations and a knockout (KO) phenotype^[12,13]. However, in-frame indels in *RHO* can cause photoreceptor degeneration via gain-of-function phenotypes such as rhodopsin misfolding or instability^[12,13].

In contrast, the HDR pathway utilizes a homologous DNA sequence as a template for repairing double-stranded break sites^[14]. In experimental settings, the homologous template sequence can be specifically designed donor sequences of interest, allowing the introduction of novel DNA sequences. Hence, accurate gene repair can be carried out utilizing the HDR pathway^[15].

A previous study has shown that heterozygous *Rho* KO mice do not develop RD^[16], although they have half the normal complement of *Rho*, and their photoreceptor OS are shorter compared to wildtype (WT) controls^[16]. Furthermore, parents of human patients with autosomal recessive RP caused by *RHO* null alleles (i.e., heterozygous carriers) do not develop RP, although they have slightly reduced rod sensitivity^[7,17]. Thus, phenotypes associated with single *RHO* null alleles are significantly milder than the phenotypes associated

with adRP *RHO* alleles.

Therefore, a gene-based treatment strategy for autosomal dominant disease involving genes such as *RHO* that do not have an associated haploinsufficiency disorder is to develop allele-specific therapeutics that knock out the mutant allele, leaving the endogenous WT allele unaffected^[18]. Another potential solution is to replace the mutant gene with an exogenous WT copy. In this paper, we introduce and characterize an *X. laevis* model of adRP caused by a mutation in the *Rho.L* gene developed by our research group, and subsequently use it to model treatments of these types. We explore three different CRISPR-based gene-editing strategies to prevent RD, in which CRISPR/Cas9 can efficiently induce double-stranded breaks resulting in pan-retinal genomic alterations. First, we use a single sgRNA to target and introduce indels into the mutant *Rho.L* allele. Second, we use a pair of sgRNAs targeting the mutant *Rho.L* allele and an upstream sequence to introduce large inactivating deletions in the mutant allele. Third, we use a single sgRNA targeting the mutant *Rho.L* allele and a single-stranded DNA oligonucleotide repair template to restore the mutant allele. Each approach is designed to have minimal effects on the remaining WT allele, ideally converting the phenotype to that of a heterozygous null (1 and 2) or WT (3). Our system may provide insight into the potential of these therapeutic approaches by illustrating an idealized scenario of very high editing efficiency combined with very early treatment.

METHODS

In-vitro transcription of sgRNA

Procedures were essential, as previously described^[19]. Briefly, oligonucleotides corresponding to sgRNA variable regions were cloned into the PDR274 vector (Addgene 42250, gift of Keith Joung). SgRNAs were *in vitro* transcribed from plasmids containing inserts of interest using the HiScribe *in vitro* transcription kit (New England Biolabs), purified using the miRNeasy kit (Qiagen), quantified using a Nanodrop spectrophotometer, assessed for integrity by agarose gel electrophoresis, and stored at -80 °C prior to use.

Gene editing

Microinjections were performed according to the methods described by Feehan *et al.*^[12], except that Cas9 protein (New England Biolabs) was used in place of Cas9 mRNA. Briefly, a WT/ *Rho.L*Δ11Δ1 female *X. laevis* was injected with human chorionic gonadotropin (HCG) to induce ovulation. Oocytes were fertilized *in vitro* using sperm from an HCG-primed WT male. Utilizing a Hamilton syringe pump with continuous flow (36 μL/h), plates of ~125 embryos were injected with mixtures of one or two sgRNAs (0.5 μL of each guide at 875 ng/μL), Cas9 protein (0.5 μL at 20 μM), 0.25 μL eGFP (enhanced green fluorescent protein) mRNA and nuclease-free H₂O to make a final volume of 2.5 μL. Each embryo was injected for 1 s, equating to 20 nL of editing reagent mixture. At 36 h post-fertilization, successfully injected embryos were identified by eGFP fluorescence using an epifluorescence-equipped Leica MZ16F microscope.

Animal husbandry

Embryos were housed in glass dishes in an 18 °C incubator on a 12 h dark: 12 h light cycle. Embryos and tadpoles were reared in 10 mM NaCl, 0.2 mM KCl, 0.1 mM MgCl₂, 0.2 mM CaCl₂. Post-metamorphic frogs were raised in 10 mM NaCl.

Dot blot assay, immunohistochemical labeling and confocal microscopy

At 14 days post fertilization (dpf) (developmental stage 48) normally developed tadpoles were sacrificed by pithing. The left eye was solubilized in 100 μL of a 1:1 mixture of phosphate-buffered saline and SDS-PAGE loading buffer containing 1 mM ethylenediaminetetraacetic acid and 100 μg/mL phenylmethylsulfonyl fluoride, while the contralateral eye was fixed in 4% paraformaldehyde buffered with 0.1 M sodium phosphate pH 7.4. Dot blot assays were performed on solubilized eyes as described by Tam *et al.*^[20] and

probed with anti-rod opsin antibodies mAbB630N or mAb514-18 (at 1:10 dilution of tissue culture supernatant, gifts of W.C. Smith). The mAbB630N epitope is contained within residues 3-14^[21], while the epitope for mAb514-18 includes residue F13 found in mammalian rod opsins^[22]. Secondary antibody was IR-dye800-conjugated goat anti-mouse used at 1:10000 of 1 mg/mL solution (LI-COR Biosciences). A LI-COR Odyssey imaging system was used to image and quantify blot signals. Samples were prepared for confocal microscopy as previously described^[23]. Fixed eyes were infiltrated with 20% sucrose for 48 h, embedded in OCT (Sakura Finetek), frozen, and stored at -80 °C for sectioning. 12 µM slices were cut using a cryostat and labeled overnight with mAb B630N or mAb2B2^[24] antibodies (1:10 dilution of tissue culture supernatant, mAb2B2 gift of Robert Molday). Similar to mAb514-18, mammalian rod opsin residue F13 is a critical component of the mAb2B2 epitope^[22]. Secondary antibody was Cy3-conjugated anti-mouse antibody (1:750 dilution, Jackson ImmunoResearch). Sections were counterstained with AlexaFluor 488-conjugated wheat germ agglutinin (WGA; Life Technologies) and Hoechst 33342 (Sigma-Aldrich) and imaged using a Zeiss 800 laser scanning confocal microscope with a 40X NA 1.2 water immersion objective. Adobe Photoshop was used for post-processing and figure assembly. In order to improve image detail, non-linear adjustments were performed on Hoechst 33342 and WGA labeling channels. Antibody signal was linearly adjusted for better visualization.

Genomic DNA extraction, PCR, and sequencing

We designed four PCR primers to specifically amplify *Rho.L* regions of interest without amplifying other *X. laevis* *Rho* genes [Supplementary Material 1]. Genomic DNA was extracted from tadpole tail clips as previously described^[19]. Genomic DNA samples were PCR amplified and analyzed by gel electrophoresis. PCR products were treated with an exoSAP protocol^[25] and Sanger sequenced using a commercial service (Genewiz).

Electroretinogram recordings

Electroretinograms (ERGs) were recorded from dark-adapted animals at age 9 months as previously described^[26]. Following the recordings, blood samples were collected to identify genotypes (WT vs. WT/*Rho.LΔ11Δ1*) via Sanger sequencing. An example of analysis is shown in Supplementary Material 2.

Statistical analyses

GraphPad Prism software (version 9.0.0) was used to perform statistical analyses and generate figures. Specific tests and numbers of animals used are given for each experiment in the results section.

RESULTS

In a previously published study^[12], we used CRISPR/Cas9 to generate indels in the *X. laevis* *Rho* genes. We determined that *X. laevis* have three *Rho* genes (*Rho.L*, *Rho.2.L*, and *Rho.S*), and that in-frame indels in the *X. laevis* *Rho* genes cause RD, while frame-shifting indels have minimal phenotype. From this initial set of animals, we identified a line carrying a complex deletion comprised of adjacent 11bp and 1bp deletions that immediately follow the start codon of the *Rho.L* gene. The complex deletion could be formally designated Chr4L:131405006_131405016delAACGGAACAGA,131405030delT using HVGS nomenclature, but is hereafter referred to as “*Rho.LΔ11Δ1*” [Figure 1A, Supplementary Materials 1 and 3]. Preliminary data derived from *X. laevis* *Rho.L* knockout tadpoles [Supplementary Material 4] suggests that *Rho.L* is the highest expressing of the three *X. laevis* *Rho* genes, and that each *Rho.L* allele contributes no more than 42% to the total retinal rod opsin.

Initial characterization of the *Rho.LΔ11Δ1* *X. laevis* model for adRP

We characterized *X. laevis* tadpoles aged 14 dpf generated from a cross between WT and heterozygous WT/*Rho.LΔ11Δ1* animals. Genotypically, the offspring were expected to be half WT and half WT/*Rho.LΔ11Δ1*. A

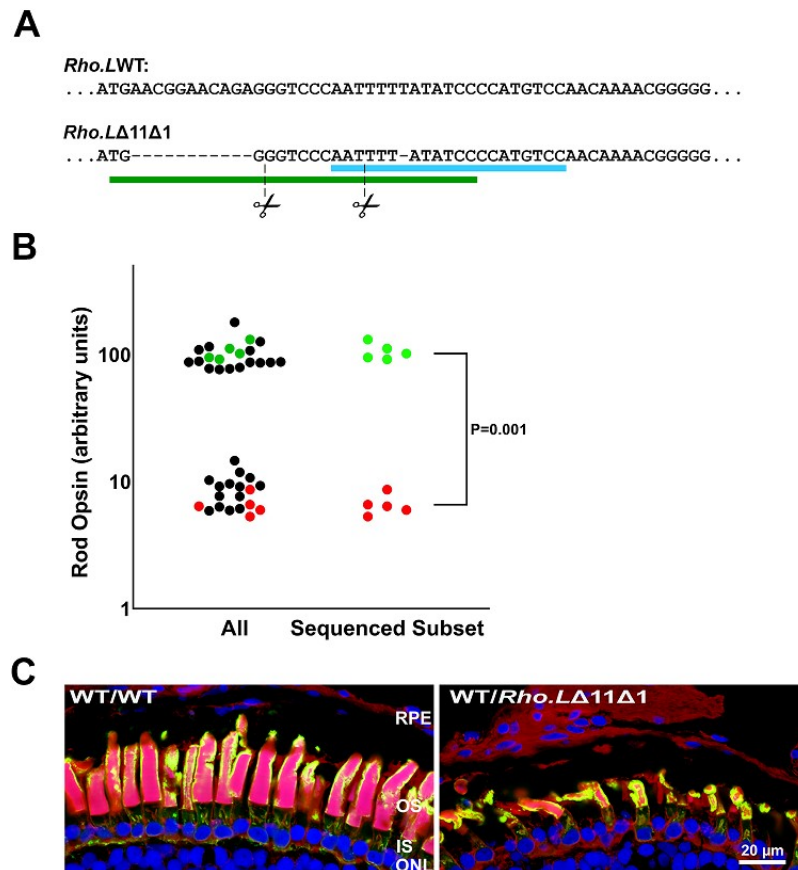


Figure 1. Characterization of a new *X. laevis* adRP model. (A) *Rho.L* WT and *Rho.LΔ11Δ1* sequences, beginning with the translation start site. The deleted (11 + 1) bases are indicated with dashes. The Sg6 target site is underlined in green. The Sg5 target site is underlined in blue. Corresponding predicted cut sites are indicated by scissors icons. (B) Dot blot assay for total rod opsin in a population derived from a mating between WT and WT/*Rho.LΔ11Δ1* genotypes shows that two distinct groups are present with high and low rod opsin levels. Detection was with mAbB630N. Each data point represents a different animal. Five animals with high rod opsin levels and five with low rod opsin levels were genotyped (colored dots). Green were identified as WT, red were identified as WT/*Rho.LΔ11Δ1*. Black: not genotyped. (C) Confocal micrographs comparing retinal structure between WT and WT/*Rho.LΔ11Δ1* genotypes. RD was observed in WT/*Rho.LΔ11Δ1* animals relative to WT. Green: mabB630N (rod opsin); red: WGA; blue: Hoechst dye.

dot blot assay indicated markedly lower levels of rod opsin ($6.6\% \pm 0.6\%$) in half the tadpole eyes [Figure 1B]. Five subjects with high rod opsin levels and five with low rod opsin levels were randomly selected and genotyped by Sanger sequencing. All five animals with high rod opsin levels were WT (green data points, Figure 1B) while all five animals with low rod opsin levels were WT/*Rho.LΔ11Δ1* (red data points, Figure 1B). The results indicate that the low rod opsin phenotype is associated with the WT/*Rho.LΔ11Δ1* genotype ($P = 0.001$, chi-squared test). Based on results shown in Supplementary Material 4, one would expect > 50% of Rho remaining in heterozygous animals with a single functional allele. In the case of our adRP model, the very low rod opsin levels apparent by dot blot ($6.6\% \pm 0.6\%$ of WT) indicate a dominant RD phenotype in heterozygous WT/*Rho.LΔ11Δ1* animals.

Note that it is likely that the mAbB630N antibody used in these assays does not detect the mutant protein, as the epitope is located at residues 3-14^[21] and residues 2-8 are missing or altered by the *Rho.LΔ11Δ1* deletion. However, western blot experiments using the anti-rod opsin C-terminal antibody mAb11D5 indicated that the mutant protein is present at very low levels relative to the WT protein (not shown). Therefore it is unlikely that the dot blot assay significantly underreports rod opsin levels in these animals.

Immunohistochemical labeling and confocal microscopy of contralateral eyes from genotyped tadpoles further demonstrated that low rod opsin levels were due to an RD phenotype. In WT animals, healthy retinas were observed with extended Rho-expressing rods and rod outer segments. In contrast, WT/*Rho.LΔ11Δ1* animals had significant RD apparent by confocal imaging, with disturbed and shortened rod outer segments [Figure 1C].

sgRNA design

In order to target precise regions within *Rho.L*, we designed and generated sgRNAs as previously described^[12]. We identified 20bp target sequences adjacent to PAM sites appropriate for CRISPR editing [Supplementary Material 1]. We identified two target sites that incorporate the *Rho.LΔ11Δ1* mutation sequence in exon 1 (Sg5 and Sg6). In addition, we identified one site 1218 bp upstream of the start codon in a less-conserved upstream promoter region of *Rho.L* that was not found in *Rho.2.L* or *Rho.S* (Sg2). In order to guard against off-target effects, we confirmed that the Sg2, Sg5, and Sg6 target sites were unique by using nblast to scan the *X. laevis* genome sequence available online at Xenbase.org^[27]. Notably, the Sg5 recognition sequence only differs from WT by a single nucleotide [Figure 1A and Supplementary Material 1].

Comparing single-guide and double-guide CRISPR-based treatments

In our first experiments of gene-editing therapy in WT/*Rho.LΔ11Δ1* animals, we utilized the *Rho.LΔ11Δ1*-targeting sgRNAs (Sg5 and Sg6) either alone or in combination with the *Rho.L* promoter-targeting sgRNA (Sg2) to evaluate the utility of these therapeutic strategies and compare their efficacy. The sgRNAs, along with Cas9 protein and mRNA encoding eGFP (as a tracer to confirm successful delivery of RNA) were injected into single-cell *X. laevis* embryos derived from a WT/*Rho.LΔ11Δ1* female and a WT male. After 36 h, non-fluorescent embryos were eliminated from the experiment. At 14 dpf, the tadpoles were sacrificed, genomic DNA was collected for PCR analysis, and the animals were genotyped by Sanger sequencing. One eye was solubilized for a rod opsin dot blot assay, while the other was processed for confocal microscopy.

RD was prevented in animals treated with single and double-guide approaches

As shown in [Figure 2A and C], the single and double-guide treatments had minimal effects on WT animals, with a mild toxic effect in the case of Sg6. However, treatment of WT/*Rho.LΔ11Δ1* animals with sgRNAs targeting the *Rho.LΔ11Δ1* mutation resulted in significantly higher levels of rod opsin compared to untreated animals [Figure 2B and D]. This effect was observed with both Sg5 and Sg6 guides [untreated ($n = 9$), Sg5-treated ($n = 19$), $P = 0.000056$; untreated ($n = 11$), Sg6-treated ($n = 11$), $P = 0.0013$ by Dunn's test for multiple comparisons]. However, average rod opsin levels were still approximately 1/3 lower than WT animals. Combining the Sg5 and Sg6 guides with the Sg2 guide (targeting the upstream promoter) also resulted in higher levels of rod opsin compared to the untreated WT/*Rho.LΔ11Δ1* group, but was not superior to the single-guide approach [untreated ($n = 9$), Sg2+5-treated ($n = 10$), $P = 0.018$; untreated ($n = 11$), Sg2+6-treated ($n = 7$), $P = 0.032$ by Dunn's test for multiple comparisons]. There was no significant difference between treatments with a single guide vs. two guides.

As shown in [Figure 2E], the *Rho.LΔ11Δ1* allele results in significant RD and loss of rods. RD was prevented in animals treated with either the Sg5 or Sg6 guides. Single-guide treatment of WT embryos with Sg5 and Sg6 did not have detrimental effects, confirming the specificity of the guides for the mutant allele, as NHEJ of the WT allele would be expected to cause RD^[12].

RD was also significantly prevented in animals simultaneously treated with two sgRNAs, in both Sg2+Sg5 and Sg2+Sg6 groups. Overall, although the rod opsin levels were increased [Figure 2B and D] and RD was prevented in the group treated with two guides [Figure 2E], this treatment approach was not statistically superior to the single-guide approach.

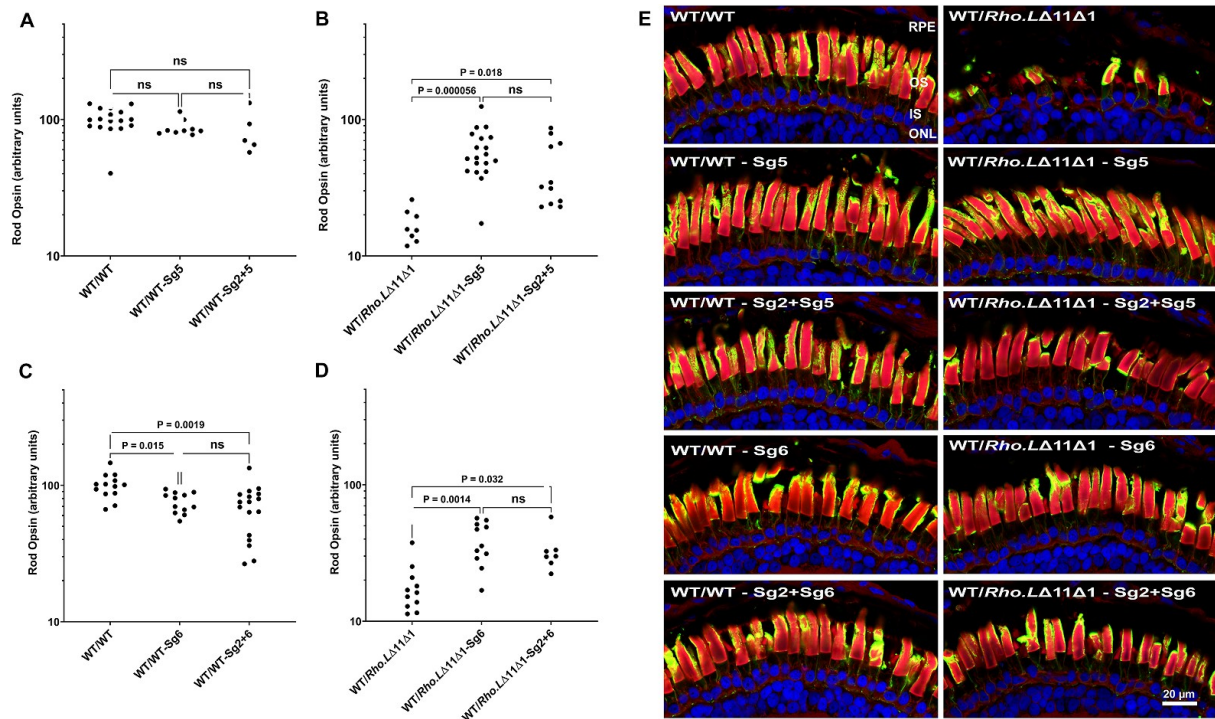


Figure 2. Single guide and double-guide treatment outcomes assayed by dot blot and confocal microscopy. (A-E) Total rod opsin levels assayed by dot blot using mabB630N anti-rod opsin antibody. Rod *P* values were determined by Kruskal-Wallis followed by Dunn's test for multiple comparisons compare groups. *P* values for Dunn's test are shown on the plots, *P* value for the Kruskal-Wallis test is given below (A) WT/WT ($n = 17$), WT/WT-Sg5 ($n = 10$), WT/WT-Sg2+5 ($n = 5$) ($P = 0.051$). (B) WT/Rho.LΔ11Δ1 ($n = 8$), WT/Rho.LΔ11Δ1-Sg5 ($n = 19$), WT/Rho.LΔ11Δ1-Sg2+5 ($n = 11$) ($P = 0.00011$). (C) WT/WT ($n = 13$), WT/WT-Sg6 ($n = 12$), WT/WT-Sg2+6 ($n = 17$) ($P = 0.0014$). (D) WT/Rho.LΔ11Δ1 ($n = 11$), WT/Rho.LΔ11Δ1-Sg6 ($n = 11$), WT/Rho.LΔ11Δ1-Sg2+6 ($n = 7$) ($P = 0.0011$). (E) Significant RD observed in Rho.LΔ11Δ1 animals relative to WT was prevented in groups treated with single and double guides, while no RD was observed in treated WT animals. Confocal micrographs are from representative retinas from each group. Green: mabB630N (rod opsin); red: WGA; blue: Hoechst dye.

For all treatments, Sanger sequencing traces showed evidence of editing of the *Rho.LΔ11Δ1* allele (example shown in [Supplementary Material 2](#)).

Simultaneous treatment with Sg2 and Sg5 resulted in large deletions in 6 out of 11 cases

The novel approach of attempting to knock out a mutant gene by inducing DSBs on both sides of the mutant allele start codon was successfully carried out in over half of the WT/Rho.LΔ11Δ1 animals simultaneously injected with Sg2 and Sg5. In those animals, a 1248bp DNA fragment between the Sg2 and Sg5 recognition sites containing the *Rho.L* transcription start site and start codon was removed. This large edit was verified via PCR product sizes on 1% agarose gels [[Figure 3A](#)] and Sanger sequencing [[Figure 3B](#)]. Animals with large deletions were protected from RD [[Figure 3C](#)]. However, as noted above, the overall histological outcomes and protein levels were not significantly improved by this approach relative to the single-guide approach.

Editing a non-conserved region of the *Rho.L* promoter does not cause RD

In a separate experiment, we looked for detrimental effects NHEJ induced by the upstream sgRNA might have on the function of WT alleles. We injected WT embryos with Cas9 and Sg2. A dot blot assay demonstrated no difference in rod opsin content in retinas from un-injected and Sg2-injected WT tadpoles, suggesting that minor disruptions of the promoter region caused by Sg2 editing do not affect rhodopsin levels ($n = 15$ per group; Mann Whitney *U* test, [Figure 3D](#)). Additionally, retinas of Sg2-injected WT

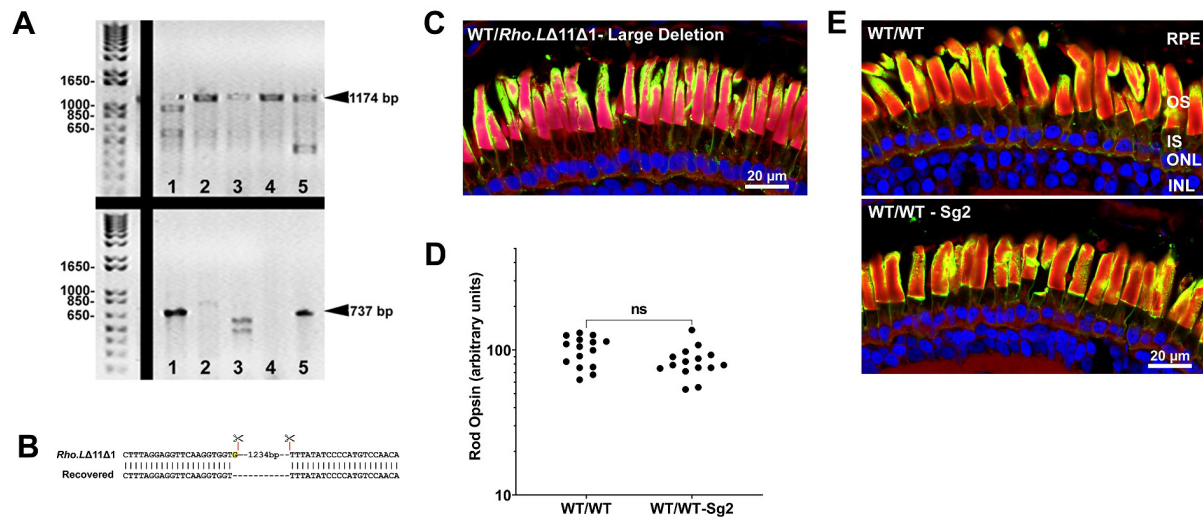


Figure 3. Double-guide treatment causes large deletions that prevent RD in WT/*Rho.LΔ11Δ1* animals. (A) Agarose gel electrophoresis analysis of PCR products. Top row shows PCR products amplified using primers 2 and 4 [Supplementary Material 1] that are 1174 bases apart. The presence of the 1174 bp product indicates genomic DNA that does not contain large deletions. Bottom row contains PCR products amplified using the same genomic DNA samples with primers 1 and 4 [Supplementary Material 1], which are 1971 bases apart. Our standard PCR conditions do not efficiently amplify the full-length PCR product. Bands at 737 bp in this row indicate the presence of large deletions. Darker 737 bp bands in the bottom row in lanes 1 and 5 as well as the respective lighter 1174 bp bands in the top row indicate that the large deletion likely occurred to a greater extent in samples 1 and 5. Sample 4 is an example of a WT/*Rho.LΔ11Δ1* animal treated with Sg2+Sg5, in which a large deletion was not introduced successfully. Markers are 1kb ladder (New England Biolabs). (B) Example sequence of a large deletion induced by editing with Sg2 and Sg5. The upper sequence shows the sequences of the *Rho.LΔ11Δ1* allele that flank the Sg2 and Sg5 predicted cut sites (illustrated by vertical red lines and scissors icons), with 1234bp of intervening sequence between the cut sites (not shown). Sequences recovered from PCR products (the lower sequence is an example) are consistent with large deletions caused by editing with Sg2 and Sg5. In the example shown, the intervening 1234 bp is missing, as well as one additional guanine nucleotide. This sequence was recovered from the sample shown in lane 1 above. (C) Representative confocal micrograph from a WT/*Rho.LΔ11Δ1* animal treated simultaneously with Sg2 and Sg5, in which a large inactivating deletion was detected. Green: mabB630N (rod opsin); red: WGA; blue: Hoechst dye. (D) Dot blot analysis for rod opsin of WT/WT animals treated with the Sg2 guide. Rod opsin was detected with mabB630N ($n = 15$ per group; P value is from Mann-Whitney U test). (E) Confocal micrographs of retinal sections from untreated WT animals. Green: mabB630N (rod opsin); red: WGA; blue: Hoechst dye.

animals were indistinguishable from retinas of untreated controls via confocal microscopy, and we did not observe any RD [Figure 3E]. Extensive chimeric editing of the target site, the typical result of similar injections in this system^[12,27] was confirmed by Sanger sequencing of a subset of the animals ($n = 5$ from each group, not shown). (Example shown in Supplementary Material 5).

Long term functional outcomes assessed by electroretinography

Retinal degenerations are progressive disorders that, in late stages, may be driven by the altered retinal environment caused by missing photoreceptors. Therefore, a number of animals from the experiments described above were set aside and allowed to reach maturity to examine long-term outcomes. We compared rod photoreceptor function between the WT/*Rho.LΔ11Δ1* and WT/WT animals using scotopic ERG measurements. The a-wave and b-wave amplitudes were measured in response to different flash intensities. A-wave amplitude was found to be significantly reduced ($P = 0.0059$; two-way ANOVA) in *Rho.LΔ11Δ1* animals ($n = 10$) compared to the WT ($n = 6$). The average b-wave amplitude was not found to be statistically different between the two groups [Figure 4B]. The effects on a-wave were most apparent at higher flash intensities [Figure 4A].

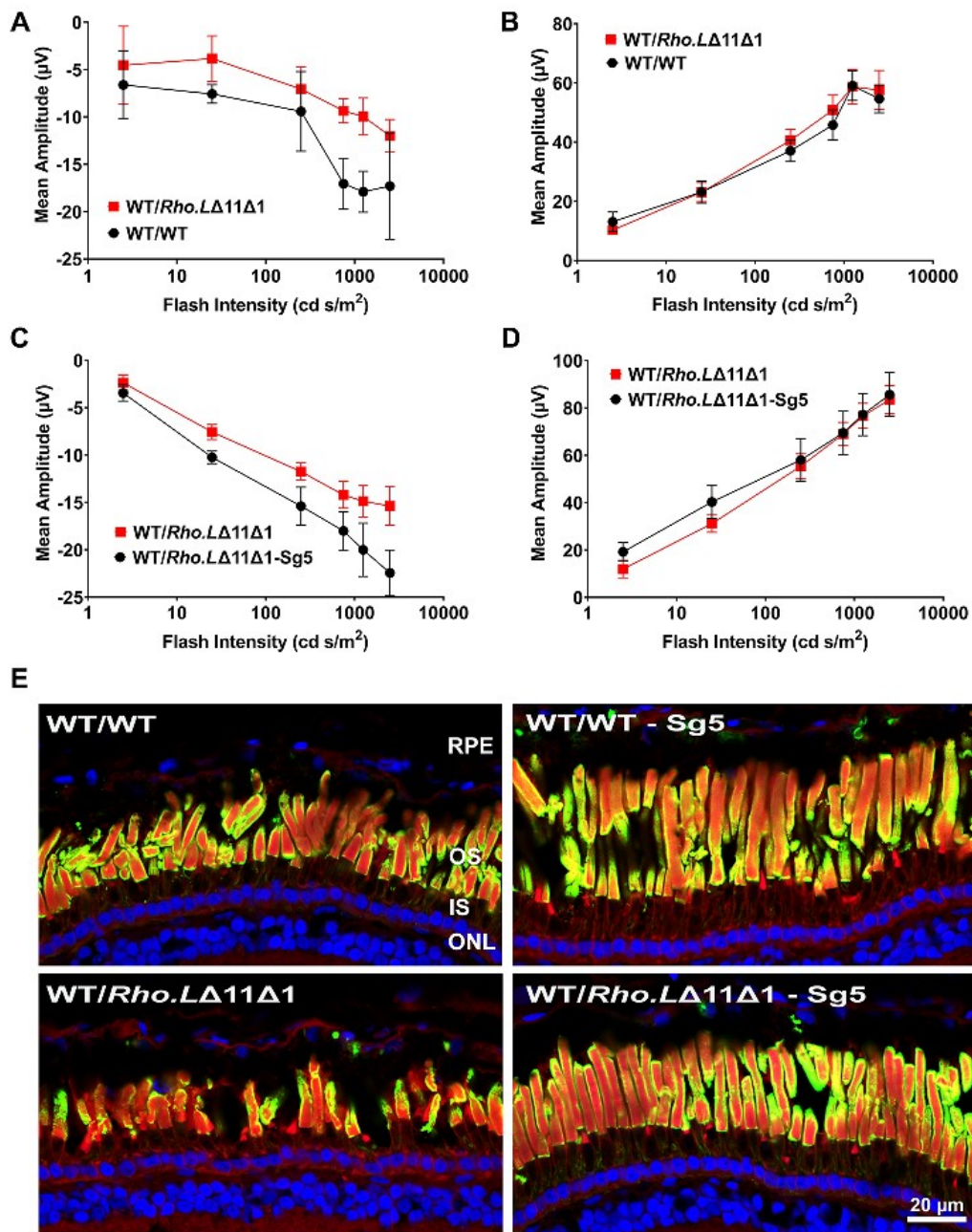


Figure 4. Electrophysiology and histology of nine-month-old animals. (A, B) WT/*Rho.LΔ11Δ1* (red, $n = 10$) comparison with WT/WT (black, $n = 6$). (A) Mean a-wave amplitude: two-way ANOVA indicates a flash intensity effect ($P = 0.0027$), and a genotype effect ($P = 0.0059$). (B) Mean b-wave amplitude: two-way ANOVA indicates a flash intensity effect ($P < 0.0001$), but no effect of genotype. (C, D) WT/*Rho.LΔ11Δ1* (red, $n = 8$) comparison with WT/*Rho.LΔ11Δ1-Sg5* (black, $n = 5$). (C) Mean a-wave amplitude: two-way ANOVA indicates a flash intensity effect ($P < 0.0001$), and a treatment effect ($P = 0.0001$). (D) Mean b-wave amplitude: two-way ANOVA indicates a flash intensity effect ($P < 0.0001$), but no effect of genotype. Data presented as mean amplitude \pm SEM in response to different light intensities. P values were determined by two-way ANOVA. (E) Confocal micrographs of retinal sections from 9-month old animals. RD is apparent in untreated 9-month-old WT/*Rho.LΔ11Δ1* animals. Sg5-treated WT/*Rho.LΔ11Δ1* animals are indistinguishable from WT animals. Green: mabB630N (rod opsin); red: WGA; blue: Hoechst dye.

Subsequently, we assessed long-term effects of the Sg5-guide treatment on retinal function in WT/*Rho.LΔ11Δ1* animals. We found no difference in mean b-wave amplitudes between the treated and untreated groups [Figure 4D]. However, mean a-wave amplitude was significantly increased ($P = 0.0001$;

two-way ANOVA) in Sg5-treated animals ($n = 5$) compared to the untreated adRP animals ($n = 8$) [Figure 4C]. Our results indicate long-term improvement in retinal function in the Sg5-treated group.

We further assessed these long-term outcomes by histology. Nine-month-old animals from untreated and Sg5-treated groups were sacrificed and genotyped. Eyes were dissected, embedded, sectioned, labeled, and imaged as previously described to assess long-term effects of the *Rho.LΔ11Δ1* mutation and gene editing treatments. As shown in [Figure 4E], significant RD and loss of rods are observed in older *Rho.LΔ11Δ1* animals. In agreement with the functional recovery seen in our ERG analysis, RD was prevented in Sg5-treated animals, again indicating long-lasting benefits of treatment.

CRISPR-mediated HDR as a treatment approach for adRP

Although knocking out the *Rho.LΔ11Δ1* allele by inducing NMD via indels introduced by NHEJ was effective in preventing RD in our animal model, we expected the strategy to be successful only in the two-thirds of photoreceptors that would carry frame-shifting mutations. In the remaining one-third of cases, in-frame mutations would be neutral or aggravating, and this is likely reflected by the total rod opsin levels in treated groups averaging about 2/3 of WT levels [Figure 2B and D]. Therefore, we attempted to utilize a CRISPR-induced HDR repair mechanism to improve treatment outcomes, as HDR should produce error-free repairs. We designed an experiment to compare the efficacy of our single-guide-based therapy to HDR-based repair. We designed a 120-nucleotide single-stranded repair template that spanned the Sg5 cut site, with the *Rho.LΔ11Δ1* sequence restored to WT; recombination would revert the *Rho.LΔ11Δ1* sequence to WT and eliminate the Sg5 target site. In addition, we included a mutation that induces the amino acid change M13F; this innocuous change generates a binding site for anti-mammalian rod opsin monoclonal antibodies 2B2 and 514-18, allowing us to identify cells that have undergone recombination by immunolabeling^[20,22]. Finally, we included a silent mutation that introduces an *ApoI* restriction site [Supplementary Material 2].

To test this strategy, we injected embryos from a WT male and a WT/*Rho.LΔ11Δ1* female with Cas9 and Sg5 alone to induce the NHEJ, or Cas9 and a combination of Sg5 and ssDNA template to induce HDR and compared them to untreated controls. The amount of ssDNA template injected (200 pg per embryo) was separately determined to be the maximum amount that could be injected without high levels of toxicity [Supplementary Material 4]. At 14 dpf, the animals were sacrificed, and genomic DNA samples were collected for PCR analysis and Sanger sequencing. One eye was solubilized for dot blot assays, while the other was fixed for confocal microscopy.

Similar to our findings in the previous experiment, both rod opsin dot blot and histology were consistent with RD in untreated heterozygous WT/*Rho.LΔ11Δ1* animals that were prevented by the Sg5 treatment (Figure 5A; $n = 32$ per group; $P = 0.017$ by Kruskal-Wallis test). Hence, the results of the previous experiment were replicated. Significant RD was also prevented in the group of animals treated with Sg5 in combination with the ssDNA repair template [Figure 5A and B]; $n = 32$ per group; $P = 0.027$ by Dunn's multiple comparisons. There was no statistically significant difference between the Sg5 and Sg5 + ssDNA treatments. The genotypes of a subset of animals were identified via Sanger sequencing (Figure 5A, colored data points). As anticipated, we found higher levels of rod opsin in WT animals compared to mutants in both treated and untreated groups. Similar to the experiment shown in [Figure 2], we observed evidence of mosaic editing by Sg5 in the sequencing traces, and no evidence of HDR repair.

HDR inefficiently repaired the *Rho.LΔ11Δ1* allele

In order to assess the efficiency of HDR in the 36 animals treated with Sg5 + ssDNA, three different assays were carried out: (1) *Rho.L* exon 1 was amplified by PCR from each animal, and restriction analysis was

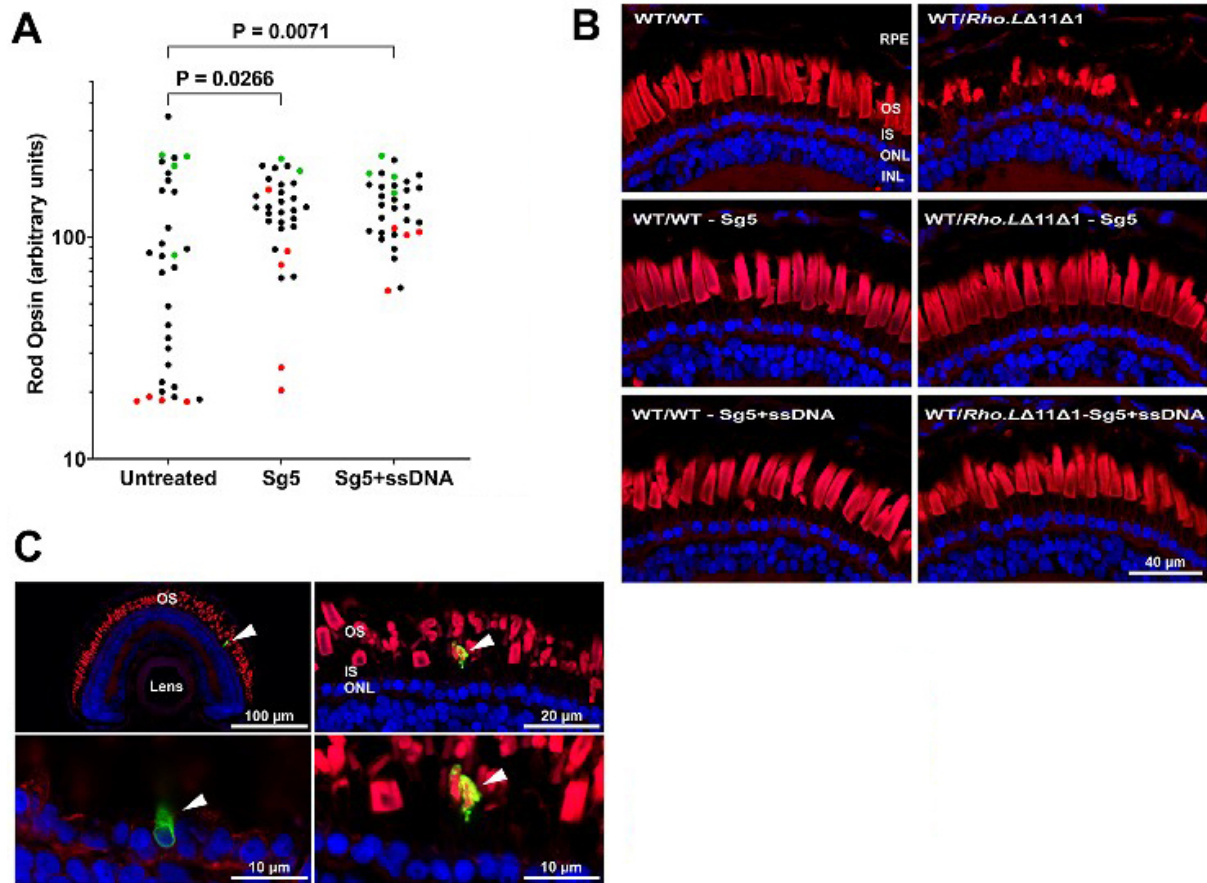


Figure 5. Comparison of HDR and NHEJ-based treatments. (A) Total rod opsin levels assayed by dot blot using mabB630N antibody. The genotypes of a subset of animals were determined by Sanger sequencing. Green: WT/WT, red: derived from WT/Rho.LΔ11Δ1, black: not sequenced. *P* values were determined by Kruskal-Wallis followed by Dunn's multiple comparisons test ($n = 32$ per group). For the Kruskal Wallis test, $P = 0.017$; values for Dunn's tests are shown on the plot. (B) Confocal micrographs of retinal sections from corresponding untreated, Sg5-treated, and Sg5+ssDNA treated animals. RD observed in WT/Rho.LΔ11Δ1 animals was prevented in both treatment groups. Red: WGA; blue: Hoechst dye. (C) Confocal micrograph showing a mab2B2-positive cell, indicating successful homologous recombination of the ssDNA template. The single cell indicated by the arrowheads is shown at several magnifications. The bottom panels show different optical sections focused on the inner and outer segments, respectively. Green: mab2B2; Red: WGA; blue: Hoechst dye.

used to detect the novel *ApoI* restriction site included in the ssDNA repair template. However, we were unable to detect any *ApoI* cleavage. (2) A second dot blot assay was probed with anti-mammalian rod opsin antibody mab514-18 to detect rod opsin containing the M13F point mutation that we included in the ssDNA template. However, we found no evidence of increased mab514-18 binding in this assay. (3) Retinal cryosections from all 36 animals were labeled with mab2B2 anti-mammalian rod opsin antibody and imaged using confocal microscopy. Only a single rod in one of the sections was found to be 2B2-positive [Figure 5C]. Since 2B2 labeling was not detected in any other animal, we concluded that HDR was extremely inefficient. Considering the lack of evidence for HDR repair from multiple modes of testing, we concluded that the improved phenotype in the Sg5-ssDNA treated group was likely due to the NHEJ mechanism induced by the Sg5 edit and not HDR.

DISCUSSION

In this study, we have described a new *X. laevis* model for adRP, for which we have demonstrated utility for testing CRISPR-based gene editing strategies as treatment approaches. This model, which carries a 12 bp

deletion in the *Rho.L* gene, was previously developed in our laboratory using the CRISPR/Cas9 gene editing system^[12]. The in-frame deletion in the first exon of the *X. laevis Rho.L* gene results in a dominant RD phenotype that is likely caused by defects in the biosynthesis of Rho protein, similar to previously described mutations associated with adRP in humans (e.g., P23H)^[28,29]. In support of this, we were unable to convincingly detect the truncated mutant protein in the background of WT rod opsin by western blot using the anti-C-terminal antibody mab11D5 (not shown). Successful gene editing therapies in this model have similar requirements to those for human autosomal dominant disease, in that the mutant allele would either need to be eliminated or restored^[18]. Thus, this model provides us with the means to rapidly survey a variety of gene-editing treatment strategies for adRP. Due to the relative ease of gene editing in embryonic *X. laevis*, the therapies were uncomplicated by issues such as delivery to the retina, or timing of delivery, both currently the subject of extensive research. Therefore, our experiments model idealized scenarios in which these issues have been solved.

Treating animals with a single sgRNA uniquely targeting the *Rho.L* Δ 11 Δ 1 allele was overwhelmingly successful. We expected NHEJ to result in out-of-frame mutations and nonsense-mediated decay in approximately two-thirds of photoreceptors. Hence, loss-of-function mutations in the malfunctioning alleles were projected to prevent the majority, but not all, of the RD. The treatment significantly prevented RD in almost all animals, assessed by both dot blot for rod opsin and histology. Additionally, we were able to demonstrate that a single-base discrepancy is sufficient for Cas9 to distinguish between the WT and mutant alleles. This is particularly important for potential clinical use of gene editing strategies, as the majority of adRP-associated *RHO* mutations reported in human patients are alterations of a single nucleotide. Most recently, Diakatou *et al.*^[30] have published their work using a similar editing strategy to treat G56R and NR2E3 adRP mutations in iPSCs. They designed unique sgRNAs to specifically target mutant alleles with a single-base difference and successfully utilized CRISPR/Cas9 to introduce NHEJ-mediated indels that KO the mutant allele^[30]. Latella *et al.*^[31] have also used a similar gene-editing approach in mouse retinas carrying the human P23H rhodopsin gene, through subretinal electroporation of plasmid-based Cas9. There are also limitations associated with NHEJ-based treatment for adRP. Although we have shown that Cas9 is able to discriminate minor differences between disease and WT alleles, sgRNAs cannot be designed for every known mutation due to the requirement for an adjacent PAM site. Our findings emphasize that even an imperfect treatment strategy can be highly effective.

We also tested more complex editing strategies, designed to address the non-productive third of expected in-frame edits. In attempting to restore the mutated allele to WT in our adRP model, we found that HDR is inefficient in *X. laevis* using our described protocol. Although the reasons remain unclear, similar results were also obtained by Feehan *et al.*^[12] in our laboratory. Here, we attempted to improve HDR efficiency relative to previous attempts by using a single-stranded repair template, as opposed to the double-stranded template used by Feehan *et al.*^[12]. However, HDR efficiency remained low relative to NHEJ. The incidence and efficiency of HDR-mediated repair are also reported to be low in mammalian cells. Maruyama *et al.*^[32] have reported HDR repair efficiencies ranging from 0.5% to 20%, compared to 20%-60% NHEJ-mediated repair in mouse models. To improve HDR efficiency, Lin *et al.*^[33] have proposed a novel strategy to synchronize cells into late S and G2 phases of the cell cycle, where HDR predominantly takes place. Alternatively, other research groups have attempted to suppress NHEJ by targeting components such as DNA ligase IV, forcing HDR to become the dominant repair pathway^[34,35].

We also used a gene inactivation strategy in which the transcription and translation start sites of the mutated gene were removed by introducing DSBs upstream and downstream of the *Rho.L* start codon to create large deletions. This also resulted in viable retinas without RD. Tsai *et al.*^[36] previously carried out a

similar treatment approach in human rhodopsin knock-in adRP mouse models using AAV injections. Utilizing double sgRNAs in combination with Cas9 protein, they introduced DSBs upstream and downstream from the rhodopsin gene's start codon (363 bp apart), resulting in large inactivating deletions in both alleles. Simultaneous with the elimination of the targeted gene, they enabled the expression of WT rhodopsin through an exogenous cDNA^[36]. Our treatment approach differs in that one of the sgRNAs designed to introduce the large inactivating deletion was designed to target only the mutant allele. Our second non-allele-specific sgRNA was designed to introduce an edit upstream from the promoter regulatory region, in a non-conserved region such that typical small indels would not be predicted to significantly disrupt gene function. Therefore, our strategy did not require the delivery of an exogenous *Rho* cDNA.

Although the introduction of large deletions was only detected in a subset of animals (6 out of 11 tested), this strategy could potentially be optimized and may also have significant utility in creating *X. laevis* knockout models. One contributing factor to the efficiency of simultaneous breaks may be the physical distance between the target sites. In our experiment, the sites were 1248 bp apart. Shorter or longer distances may affect the efficiency of deletion. Another factor may be the timing of editing; unless both cuts occur within a sufficiently narrow timeframe, two separate instances of NHEJ are more likely than a large deletion.

Treatment with a single mutation-specific sgRNA conferred long-term protection against RD and loss of retinal function, as late as 9 months of age, as assessed by histology and ERG. However, benefits were primarily observed in the ERG a-wave, which is associated with the phototransduction functions of photoreceptors. The b-wave is a reflection of communication between photoreceptors and bipolar and Müller cells within the inner retina^[37]. Hence, we speculate that the reduction in a-wave amplitudes in our adRP model is likely due to the reduced ability of rod photoreceptors to initiate phototransduction due to missing or dysmorphic outer segments, while the relatively unaffected b-wave amplitudes indicate that a large subset of viable rod photoreceptors remains at 9-months in WT/*Rho.LΔ11Δ1* animals. Overall, our results are consistent with functional impairment of rods in older animals that are prevented by gene editing. Evaluation of long-term outcomes is another useful feature of this system, as *X. laevis* lifespan routinely exceeds a decade in our hands.

CONCLUSION

Our results indicate that *X. laevis* can be used to rapidly model and compare therapeutic gene editing strategies for adRP. From initial experiments in the system, we conclude that although more complex editing strategies may be theoretically superior to simpler strategies, ultimately, they will lack superiority if their complexity reduces efficiency. Therapies that require multiple linked events to occur in each cell (such as two adjacent cuts within a narrow time frame, or a cut followed by recombination, or transfection with two viruses) will require increased efficiencies for these independent events in order to surpass the efficacy of theoretically inferior treatments requiring only a single step. Therefore, once the challenges of efficient delivery of gene editing therapeutics are overcome, it should be possible to develop efficacious adRP therapies based simply on NHEJ repair. There is likely merit to the idea of emphasizing the development of less complex treatment strategies.

DECLARATIONS

Acknowledgments

Thanks to Keith Joung, Robert S. Molday, W. Clay Smith, and Dusanka Deretic for supplying plasmid and antibody reagents.

Authors' contributions

Farhad Ghaseminejad Performed the experiments, wrote the manuscript, and contributed to experimental design: Ghaseminejad F

Developed protocols, assisted with experiments, and contributed to experimental design: Tam BM

Assisted with experiments, developed the *Rho.LΔ11Δ1* line, and performed the *Rho.L* knockout analysis: Chiu CN

Developed protocols, and initiated the development of the *Rho.LΔ11Δ1* line: Feehan JM

Conceived of the study, obtained funding, and edited the manuscript: Moritz OL

Availability of data and materials

Not applicable.

Financial support and sponsorship

This study was funded by the Canadian Institutes of Health Research (PJT-155937 and PJT-156072) and the National Science and Engineering Research Council (RGPIN-2020-05193). Ghaseminejad F was the recipient of a scholarship from the Canadian Institutes of Health Research (Canada Graduate Scholarships - Master's Program).

Conflicts of interest

All authors declared that there are no conflicts of interest.

Ethical approval and consent to participate

These studies were approved by the UBC animal care committee, certificates A18-0259 and A18-0257. Our experiments conformed to the ARVO statement for the use of animals in ophthalmic and vision research.

Consent for publication

Not applicable.

Copyright

© The Author(s) 2022.

REFERENCES

1. Hamel C. Retinitis pigmentosa. *Orphanet J Rare Dis* 2006;1:40. DOI PubMed PMC
2. Retinitis pigmentosa. Fighting Blindness Canada (FBC). Available from: <https://www.fightingblindness.ca/eye-diseases-pathways/retinitis-pigmentosa/> [Last accessed on 12 Jan 2022].
3. Verbakel SK, van Huet RAC, Boon CJF, et al. Non-syndromic retinitis pigmentosa. *Prog Retin Eye Res* 2018;66:157-86. DOI PubMed
4. Daiger SP, Sullivan LS, Bowne SJ. Genes and mutations causing retinitis pigmentosa. *Clin Genet* 2013;84:132-41. DOI PubMed PMC
5. Hartong DT, Berson EL, Dryja TP. Retinitis pigmentosa. *Lancet* 2006;368:1795-809. DOI PubMed
6. Athanasiou D, Aguila M, Bellingham J, et al. The molecular and cellular basis of rhodopsin retinitis pigmentosa reveals potential strategies for therapy. *Prog Retin Eye Res* 2018;62:1-23. DOI PubMed PMC
7. Rosenfeld PJ, Cowley GS, McGee TL, Sandberg MA, Berson EL, Dryja TP. A null mutation in the rhodopsin gene causes rod photoreceptor dysfunction and autosomal recessive retinitis pigmentosa. *Nat Genet* 1992;1:209-13. DOI PubMed
8. Hsu PD, Lander ES, Zhang F. Development and applications of CRISPR-Cas9 for genome engineering. *Cell* 2014;157:1262-78. DOI PubMed PMC
9. Jinek M, Chylinski K, Fonfara I, Hauer M, Doudna JA, Charpentier E. A programmable dual-RNA-guided DNA endonuclease in adaptive bacterial immunity. *Science* 2012;337:816-21. DOI PubMed PMC
10. Wang D, Zhang C, Wang B, et al. Optimized CRISPR guide RNA design for two high-fidelity Cas9 variants by deep learning. *Nat Commun* 2019;10:4284. DOI PubMed PMC
11. Zaboikin M, Zaboikina T, Freter C, Srinivasakumar N. Non-homologous end joining and homology directed DNA repair frequency of double-stranded breaks introduced by genome editing reagents. *PLoS One* 2017;12:e0169931. DOI PubMed PMC
12. Feehan JM, Chiu CN, Stanar P, Tam BM, Ahmed SN, Moritz OL. Modeling dominant and recessive forms of retinitis pigmentosa by editing three rhodopsin-encoding genes in *Xenopus laevis* using Crispr/Cas9. *Sci Rep* 2017;7:6920. DOI PubMed PMC

13. Zelinka CP, Sotolongo-Lopez M, Fadool JM. Targeted disruption of the endogenous zebrafish rhodopsin locus as models of rapid rod photoreceptor degeneration. *Mol Vis* 2018;24:587-602. [PubMed](#) [PMC](#)
14. Ferreira MG, Cooper JP. Two modes of DNA double-strand break repair are reciprocally regulated through the fission yeast cell cycle. *Genes Dev* 2004;18:2249-54. [DOI](#) [PubMed](#) [PMC](#)
15. Arnoult N, Correia A, Ma J, et al. Regulation of DNA repair pathway choice in S and G2 phases by the NHEJ inhibitor CYREN. *Nature* 2017;549:548-52. [DOI](#) [PubMed](#) [PMC](#)
16. Lem J, Krasnoperova NV, Calvert PD, et al. Morphological, physiological, and biochemical changes in rhodopsin knockout mice. *Proc Natl Acad Sci U S A* 1999;96:736-41. [DOI](#) [PubMed](#) [PMC](#)
17. Kartasmita A, Fujiki K, Iskandar E, Sovani I, Fujimaki T, Murakami A. A novel nonsense mutation in rhodopsin gene in two Indonesian families with autosomal recessive retinitis pigmentosa. *Ophthalmic Genet* 2011;32:57-63. [DOI](#) [PubMed](#)
18. Meng D, Ragi SD, Tsang SH. Therapy in rhodopsin-mediated autosomal dominant retinitis pigmentosa. *Mol Ther* 2020;28:2139-49. [DOI](#) [PubMed](#) [PMC](#)
19. Feehan JM, Stanar P, Tam BM, Chiu C, Moritz OL. Generation and analysis of *Xenopus laevis* models of retinal degeneration using CRISPR/Cas9. *Methods Mol Biol* 2019;1834:193-207. [DOI](#) [PubMed](#)
20. Tam BM, Xie G, Oprian DD, Moritz OL. Mislocalized rhodopsin does not require activation to cause retinal degeneration and neurite outgrowth in *Xenopus laevis*. *J Neurosci* 2006;26:203-9. [DOI](#)
21. Adamus G, Zam ZS, Arendt A, Palczewski K, McDowell JH, Hargrave PA. Anti-rhodopsin monoclonal antibodies of defined specificity: Characterization and application. *Vision Res* 1991;31:17-31. [DOI](#) [PubMed](#)
22. Tam BM, Moritz OL. Characterization of rhodopsin P23H-induced retinal degeneration in a *Xenopus laevis* model of retinitis pigmentosa. *Invest Ophthalmol Vis Sci* 2006;47:3234-41. [DOI](#) [PubMed](#)
23. Tam BM, Noorwez SM, Kaushal S, Kono M, Moritz OL. Photoactivation-induced instability of rhodopsin mutants T4K and T17M in rod outer segments underlies retinal degeneration in *X. laevis* transgenic models of retinitis pigmentosa. *J Neurosci* 2014;34:13336-48. [DOI](#) [PubMed](#) [PMC](#)
24. Hicks D, Molday RS. Differential immunogold-dextran labeling of bovine and frog rod and cone cells using monoclonal antibodies against bovine rhodopsin. *Exp Eye Res* 1986;42:55-71. [DOI](#) [PubMed](#)
25. BioTechniques - a simple way to treat PCR products prior to sequencing using ExoSAP-IT®. Available from: <http://www.biotechniques.com/BiotechniquesJournal/2008/May/A-Simple-Way-to-Treat-PCR-Products-Prior-to-Sequencing-Using-ExoSAP-IT/biotechniques-45295.html> [Last accessed on 12 Jan 2022].
26. Bocchero U, Tam BM, Chiu CN, Torre V, Moritz OL. Electrophysiological changes during early steps of retinitis pigmentosa. *Invest Ophthalmol Vis Sci* 2019;60:933-43. [DOI](#) [PubMed](#)
27. Karimi K, Fortriede JD, Lotay VS, et al. Xenbase: a genomic, epigenomic and transcriptomic model organism database. *Nucleic Acids Res* 2018;46:D861-8. [DOI](#) [PubMed](#) [PMC](#)
28. Wen RH, Stanar P, Tam B, Moritz OL. Autophagy in *Xenopus laevis* rod photoreceptors is independently regulated by phototransduction and misfolded RHO^{P23H}. *Autophagy* 2019;15:1970-89. [DOI](#) [PubMed](#) [PMC](#)
29. Tam BM, Moritz OL. Dark rearing rescues P23H rhodopsin-induced retinal degeneration in a transgenic *Xenopus laevis* model of retinitis pigmentosa: a chromophore-dependent mechanism characterized by production of N-terminally truncated mutant rhodopsin. *J Neurosci* 2007;27:9043-53. [DOI](#) [PubMed](#) [PMC](#)
30. Diakoutou M, Dubois G, Erkilic N, Sanjurjo-Soriano C, Meunier I, Kalatzis V. Allele-specific knockout by CRISPR/Cas to treat autosomal dominant retinitis pigmentosa caused by the G56R mutation in NR2E3. *Int J Mol Sci* 2021;22:2607. [DOI](#) [PubMed](#) [PMC](#)
31. Latella MC, Di Salvo MT, Cocchiarella F, et al. In vivo editing of the human mutant rhodopsin gene by electroporation of plasmid-based CRISPR/Cas9 in the mouse retina. *Mol Ther Nucleic Acids* 2016;5:e389. [DOI](#) [PubMed](#) [PMC](#)
32. Maruyama T, Dougan SK, Truttmann MC, Bilate AM, Ingram JR, Ploegh HL. Increasing the efficiency of precise genome editing with CRISPR-Cas9 by inhibition of nonhomologous end joining. *Nat Biotechnol* 2015;33:538-42. [DOI](#) [PubMed](#) [PMC](#)
33. Lin S, Staahl BT, Alla RK, Doudna JA. Enhanced homology-directed human genome engineering by controlled timing of CRISPR/Cas9 delivery. *Elife* 2014;3:e04766. [DOI](#) [PubMed](#) [PMC](#)
34. Vartak SV, Raghavan SC. Inhibition of nonhomologous end joining to increase the specificity of CRISPR/Cas9 genome editing. *FEBS J* 2015;282:4289-94. [DOI](#) [PubMed](#)
35. Srivastava M, Nambiar M, Sharma S, et al. An inhibitor of nonhomologous end-joining abrogates double-strand break repair and impedes cancer progression. *Cell* 2012;151:1474-87. [DOI](#) [PubMed](#)
36. Tsai YT, Wu WH, Lee TT, et al. Clustered regularly interspaced short palindromic repeats-based genome surgery for the treatment of autosomal dominant retinitis pigmentosa. *Ophthalmology* 2018;125:1421-30. [DOI](#) [PubMed](#) [PMC](#)
37. Miller RF, Dowling JE. Intracellular responses of the Müller (glial) cells of mudpuppy retina: their relation to b-wave of the electroretinogram. *J Neurophysiol* 1970;33:323-41. [DOI](#) [PubMed](#)